

Speckle Noise Reduction and Edge-Enhancement of Coronary Plaque Tissue in Intravascular Ultrasound Image by Using Anisotropic Diffusion Filter

Takanori Koga, Eiji Uchino, Noriaki Suetake,
Genta Hashimoto, Takafumi Hiro, and Masunori Matsuzaki

Abstract—This paper describes a novel edge-preserved smoothing method with special consideration to an intravascular ultrasound (IVUS) image. An IVUS image, which is commonly used for a diagnosis of acute coronary syndromes (ACS), is very grainy due to heavy speckle noise. The speckle noise prevents not only the medical doctors' interpretation of the IVUS image, but also the processing of medical images for computer-aided diagnoses (CADs). In order to reduce the speckle noise, in this study, we propose a modification of anisotropic diffusion filter in which a diffusion strength is locally and adaptively controlled by a weighted separability of an IVUS image. The weighted separability is a modification of separability for an edge detection with special consideration to an IVUS image. Furthermore, the proposed method not only reduces a speckle noise but also effectively enhances an edge of plaque tissue in an IVUS image. The effectiveness of the proposed method is verified by the experiments using the real IVUS images.

Index Terms—acute coronary syndromes (ACS), anisotropic diffusion, edge-preserved smoothing, intravascular ultrasound (IVUS) image, speckle noise reduction, weighted separability.

I. INTRODUCTION

Recently, the computer-aided diagnoses (CADs) of medical imaging are common in the fields of medicine [1]-[4]. The CADs support medical doctors' interpretation and findings of lesion on a magnetic resonance (MR) image, a computerized tomography (CT) image, an ultrasound image, and so on. The CADs mainly contain the following processings. Those are pre-processing of a raw image, segmentation of structures, analysis of the structures, and evaluation/classification of the structures. In the pre-processing, reduction of artifacts and denoising are mainly carried out. The performance of pre-processing significantly affects the results of the latter processings.

In the case of pre-processing of intravascular ultrasound (IVUS) image [5], [6], speckle noise reduction and edge enhancement of plaque tissue are very important issues. An IVUS image is obtained by the IVUS method [7]-[9]. The

IVUS method provides a real-time cross sectional image of a coronary artery in vivo less-invasively. It is used for a diagnosis of acute coronary syndromes (ACS) [10], [11] caused by a rupture of vulnerable plaque [12], [13].

In particular, in the quantitative assessment of plaque [14], the inner and the outer boundaries of plaque and the cross-sectional area of plaque are to be extracted and evaluated precisely [15]. Medical doctors however manually extract those boundaries and evaluate the area of plaque. This extraction task is very hard for the medical doctors. This is not only because a large number of the IVUS images must be processed, but also because it is very difficult to recognize the boundaries of plaque due to a heavy blood speckle noise. For those reasons, an efficient edge-preserved smoothing method as a pre-processing for a precise plaque boundary extraction [16]-[19] and for an area segmentation of plaque [20] is strongly required.

As the representative conventional noise reduction methods, the median filters [21], morphological analysis [22], bilateral filters [23] are well-known. Those filters can reduce speckle noise, but at the same time the edge of plaque also becomes dull unexpectedly by applying those methods.

Above all methods, an anisotropic diffusion filter [24] is known as an effective edge-preserved smoothing method, and it is broadly used [24]-[29]. When applied to a natural image, the anisotropic diffusion filter not only reduces the noise but also enhances the edge of the image. However, when applied to an IVUS image, speckle noise is unexpectedly enhanced by this filter. This is because a speckle noise is similar to a texture pattern, and the edge of plaque and that of the speckle noise pattern can not be distinguished. For an effective edge-preserved smoothing by an anisotropic diffusion filter for an IVUS image, an adaptive filtering depending on the local features of an edge must be introduced.

The purpose of this study is to develop a novel edge-preserved smoothing method employing the anisotropic diffusion filter, which is controlled by a weighted separability [30] of an IVUS image. The weighted separability is a modification of a separability [31] with special consideration to an IVUS image. A separability is a kind of statistical discriminant measure, which is effective for an edge extraction on a texture image. In the proposed method, a local and adaptive filtering is executed by controlling the diffusion strength of the anisotropic diffusion filter.

The validity and the effectiveness of the proposed method

Manuscript received December 31, 2008; revised December 31, 2008.

This work was supported in part by "Knowledge Cluster Initiative," for 2004-2009, funded by Ministry of Education, Culture, Science and Technology of Japan.

T. Koga, E. Uchino and N. Suetake are with the Graduate School of Science and Engineering, Yamaguchi University, 1677-1 Yoshida, Yamaguchi 753-8512, JAPAN. phone:+81-83-933-5699; fax:+81-83-933-5273; e-mail: {koga, uchino, suetake}@ic.sci.yamaguchi-u.ac.jp

G. Hashimoto, T. Hiro and M. Matsuzaki are with the Graduate School of Medicine, Yamaguchi University, 1-1-1 Minami-kogushi, Ube 755-8505, JAPAN.

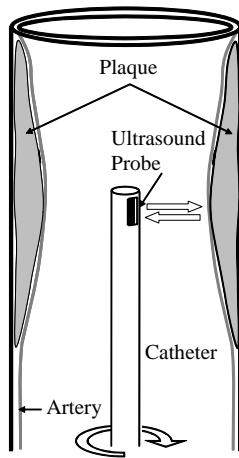


Fig. 1. An ultrasound probe attached to the distal end of a catheter.

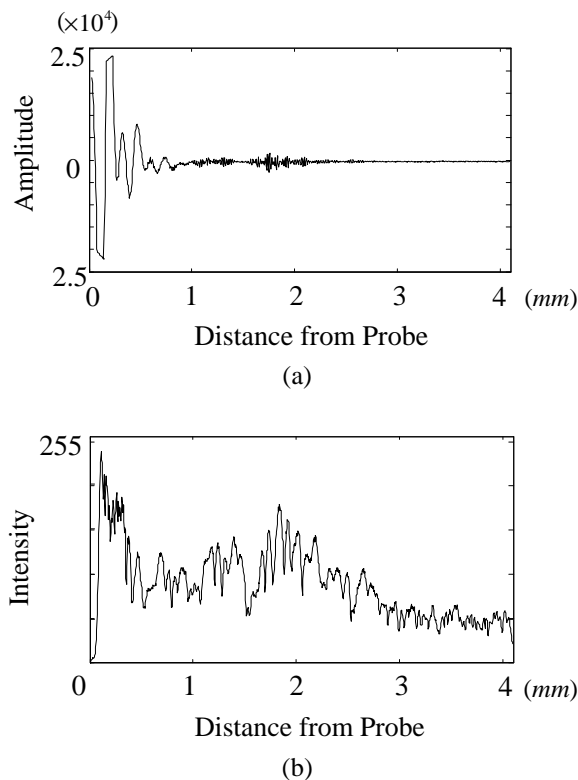


Fig. 2. Signal examples obtained by an IVUS method. (a) Sampled RF signal; (b) Luminal intensity signal of (a).

have been verified by applying it to the real IVUS images.

II. INTRAVASCULAR ULTRASOUND (IVUS) METHOD AND B-MODE IMAGE

Intravascular ultrasound (IVUS) method is one of the medical imaging techniques. It allows the application of ultrasound technology to see from inside the blood vessels out through the surrounding blood column, visualizing the inner wall of blood vessels in living individuals.

In the IVUS method, a specially designed thin catheter with a miniaturized ultrasound probe attached to its distal

end is used (see Fig.1). To visualize a coronary artery in vivo, angiographic techniques are used. The medical doctor steers the guidewire with very thin diameter from outside the body through angiography catheters into the coronary artery to be visualized. The ultrasound catheter tip is slid in over the guidewire and positioned, using angiography techniques so that the tip is at the farthest away position to be visualized. The guidewire is kept stationary and the ultrasound catheter tip is slid backwards, usually under motorized control.

The proximal end of the catheter is connected to computerized ultrasound equipment. The sound waves are emitted from the ultrasound probe, which are in the 40MHz range in this study, and the catheter also receives the reflected signal from the tissue. It is sampled at 400 MHz and stored in the computerized ultrasound equipment.

An example of a sampled radiofrequency (RF) signal is shown in Fig.2(a). An IVUS image is constructed of the amplitude information of the received RF signal. In order to visualize the inside of a coronary artery, the sampled RF signal shown in Fig.2(a) is first transformed into an 8-bit intensity signal shown in Fig.2(b) by taking the absolute value of signal, then enveloping, and finally by taking the logarithmic value. The intensity signals in all radial directions are then formed to get a tomographic cross sectional image of a coronary artery as shown in Fig.3(a).

The IVUS image shown in Fig.3(a) is called a “B-mode image.” A B-mode image displays a real time ultrasound cross-sectional image of a thin section of the blood vessel currently surrounding the catheter probe. The B-mode image is constructed with 1,024 points in depth, and 256 lines in radial direction. The resolution of distance and angle are $3.91\mu\text{m}/\text{pixel}$ and $1.41^\circ/\text{line}$, respectively.

Fig.3(b) is a B-mode image of Fig.3(a) transformed from the polar coordinates to the Cartesian coordinates. In this study, all processings are carried out in the Cartesian coordinates. Note that the aspect ratio of the IVUS image in the Cartesian coordinates is adjusted intentionally to facilitate visualization. The angle in Fig.3(b) starts from the 3-o’clock direction of the IVUS image of Fig.3(a). The vertical axis corresponds to the distance from the probe positioned at the center of the IVUS image of Fig.3(a).

In the quantitative assessment of plaque, the following two boundaries are to be extracted. One is a leading edge of a luminal boundary (LB) between the lumen and the plaque, and the other is an adventitial boundary (AB) between the plaque and the vascular wall as indicated in Fig.3(a) by the dotted lines. As a pre-processing for the boundary extraction of plaque, an edge-preserved smoothing is necessary because the plaque boundary recognition is considerably affected by heavy blood speckle noise.

III. ANISOTROPIC DIFFUSION FILTER CONTROLLED BY WEIGHTED SEPARABILITY OF IMAGE

A. Anisotropic Diffusion Filter

The anisotropic diffusion filter was originally proposed by Perona and Malik [24] in order to realize an edge-preserved

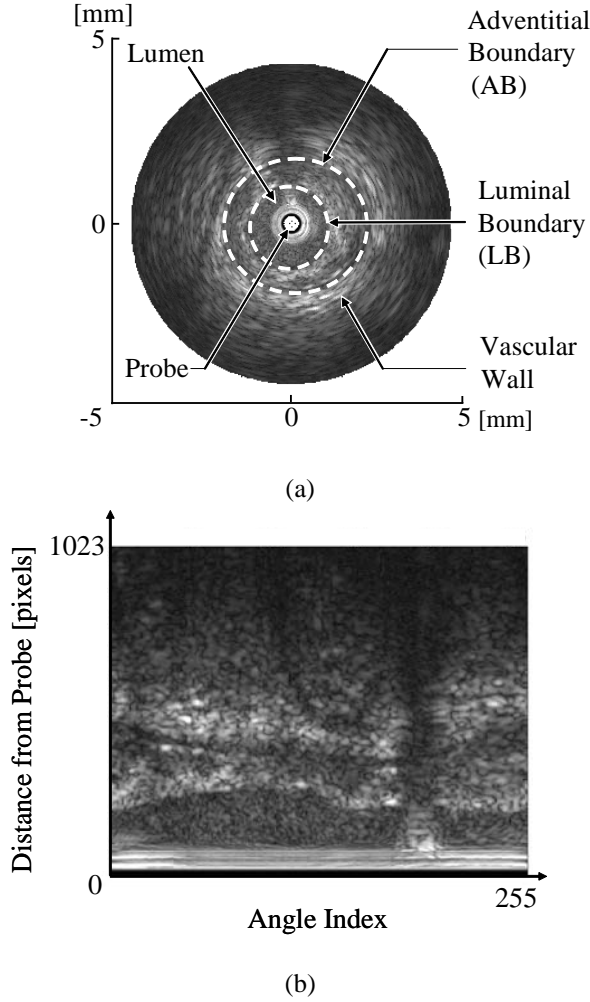


Fig. 3. IVUS B-mode image. (a) The dotted lines show a luminal boundary (LB) and an adventitial boundary (AB). (b) IVUS B-mode image transformed to the Cartesian coordinates.

smoothing for an image. In this study, Perona-Malik's Diffusion (PMD) is employed and modified to meet our needs.

The basic idea behind the PMD diffusion process is to get an increasingly smoothed image $u(x, y, t)$ from an original image $u_0(x, y)$, indexed by diffusion parameter t . This process can be interpreted as an image convolution by a Gaussian kernel with an increasing width as follows:

$$I(x, y, t) = I_0(x, y) * G(x, y, t). \quad (1)$$

The anisotropic diffusion equation is defined by:

$$\begin{aligned} I_t &= \frac{\partial I}{\partial t} = \text{div}(c(x, y, t)\nabla I) \\ &= c(x, y, t)\nabla I + \nabla c(x, y, t)\nabla I, \end{aligned} \quad (2)$$

where

$$c(x, y, t) = g(\|\nabla I(x, y, t)\|) \quad (3)$$

is a diffusion coefficient. ∇I denotes a gradient of an image. $g(\cdot)$ is called an edge stopping function, which is a decreasing function of the image. The initial condition is given by:

$$I(x, y, 0) = I_0(x, y). \quad (4)$$

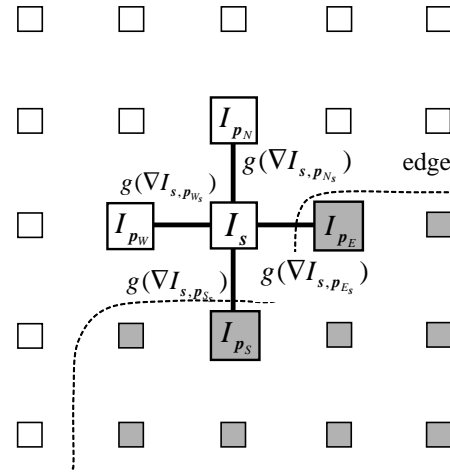


Fig. 4. Diffusion directions. An edge stopping function $g(\cdot)$ takes a small value when an intensity difference between the center pixel I_s and a neighboring pixel is large (*i.e.*, at the edge of the image).

The discrete version of PMD is given as follows:

$$I_s^{(n+1)} = I_s^{(n)} + \frac{\lambda}{|\phi_s|} \sum_{p \in \phi_s} g(\nabla I_{s,p}^{(n)}) \cdot \nabla I_{s,p}^{(n)}, \quad (5)$$

where $s=(x, y)$ and p are the coordinates of the pixel of concern and its neighboring pixels, respectively. $I_s^{(n)}$ is an intensity at s with an iteration count n . ϕ_s represents the four neighboring pixels in North, West, South and East diffusion directions as shown in Fig.4. $|\phi_s|$ is a number of the pixels in the neighborhood area, which is then $|\phi_s|=4$ in this study. λ is a parameter.

$g(\cdot)$ is called an edge stopping function. A monotonically decreasing function of the gradient of an image is usually adopted as $g(\cdot)$. The gradient of the image is calculated by:

$$\nabla I_{s,p}^{(n)} = I_p^{(n)} - I_s^{(n)}. \quad (6)$$

In PMD, the edge stopping function is given by:

$$g(z) = \frac{1}{1 + \left(\frac{z}{K}\right)^2}, \quad (7)$$

where K is a parameter which controls the strength of diffusion. $g(\cdot)$ takes large values at the regions where the intensity gradients are small. On the contrary, it takes small values at the regions where the intensity gradients are large.

The processing of PMD is performed by using the intensities of the image. Therefore, when applied to an IVUS image, not only the edges of plaque but also those of speckle patterns are both enhanced unexpectedly by this PMD processing.

B. Separability of IVUS Image

In order to distinguish the edge of plaque and that of the speckle pattern on an IVUS image, the proposed method employs a statistical discriminant measure of image separability [31]. Evaluation of image separability is very simple and has the following features:

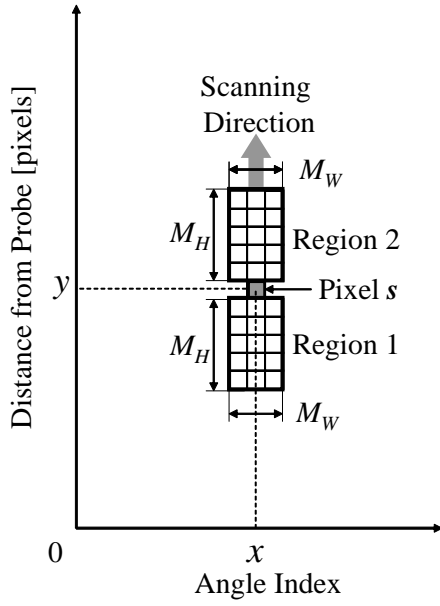


Fig. 5. Regions for calculating the image separability for a pixel $s=(x, y)$.

- 1) Robust to noisy and blurred edge,
- 2) Sensitive to detect an edge between different texture regions.

Those are the reasons why we employ image separability for a detection of plaque boundary.

Separability is calculated by a linear discriminant analysis using the information of the two local regions 1 and 2 as shown in Fig.5. The separability η_s for the pixel $s=(x, y)$ of Fig.3(b) is calculated by:

$$\eta_s = \frac{\sum_{k=1}^{k=L} \sigma_{bk}^2}{\sum_{k=1}^{k=L} \sigma_{Tk}^2}, \quad (8)$$

$$\sigma_{bk}^2 = n_1(\bar{I}_{k1} - \bar{I}_k)^2 + n_2(\bar{I}_{k2} - \bar{I}_k)^2, \quad (9)$$

and

$$\sigma_{Tk}^2 = \sum_{i=1}^{n_1+n_2} (I_{ki} - \bar{I}_k)^2, \quad (10)$$

where \bar{I}_{k1} and \bar{I}_{k2} are the means of the intensities in the regions 1 and 2, respectively. \bar{I}_k is the mean of the intensities in the combined two regions. n_1 and n_2 represent the numbers of the pixels in regions 1 and 2, respectively. η_s is $0 \leq \eta_s \leq 1$, and it takes a large value when two regions are separated with each other in the meaning of separability.

Fig.6(a) shows a discriminant image of Fig.3(b) by using η_s . Each pixel of the image represents the separability η_s . When η_s is large, high brightness is assigned to its corresponding pixel. The separability takes a large value around the regional-edge of the IVUS image. That is, a chain of white pixels with high brightness can then be a candidate of a boundary of plaque.

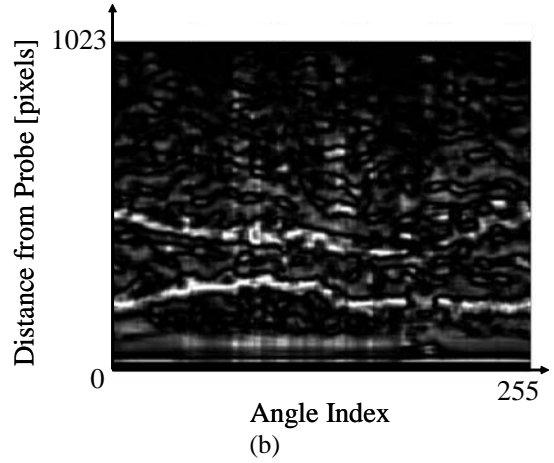
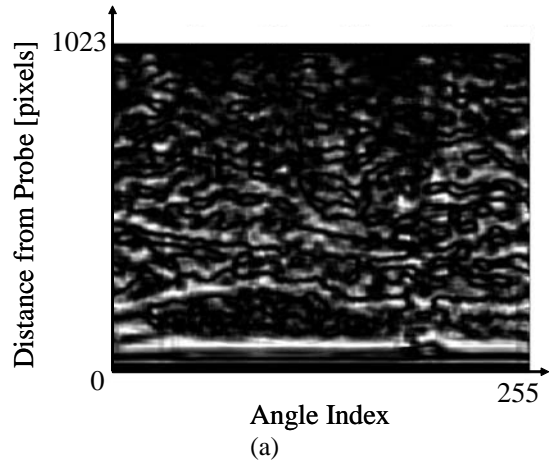


Fig. 6. (a) Discriminant image of the transformed image of Fig.3(b) by using the separability η_s with $M_W=3$ and $M_H=70$. (b) Discriminant image of the transformed image of Fig.3(b) by using the weighted separability η_s^w with $M_W=3$ and $M_H=70$.

C. Proposed Method

We propose a novel edge-preserved smoothing method in which the diffusion strength of PMD is controlled locally and adaptively by the image separability. Furthermore, the weighted separability [30] is introduced here in order to increase the edge-discriminant performance with special consideration to an IVUS image.

The weighted separability detects the candidates of the inner (lower) and the outer (upper) boundaries of plaque by considering the following two conditions peculiar to an IVUS image. Those are: 1) intensity in the outside area of a luminal boundary (LB) tends to be bigger than that in the inside area of LB; 2) intensity in the outside area of an adventitial boundary (AB) tends to be bigger than that in the inside area of AB.

For the local regions shown in Fig.5, an IVUS image is scanned from the bottom to the top. The weighted separability for a pixel s is defined by:

$$\eta_s^w = \eta_s \times \frac{(I_{MAX} - \bar{I}_1)}{I_{MAX}} \times \frac{\bar{I}_2}{I_{MAX}}, \quad (11)$$

where I_{MAX} is a maximum intensity on the whole IVUS

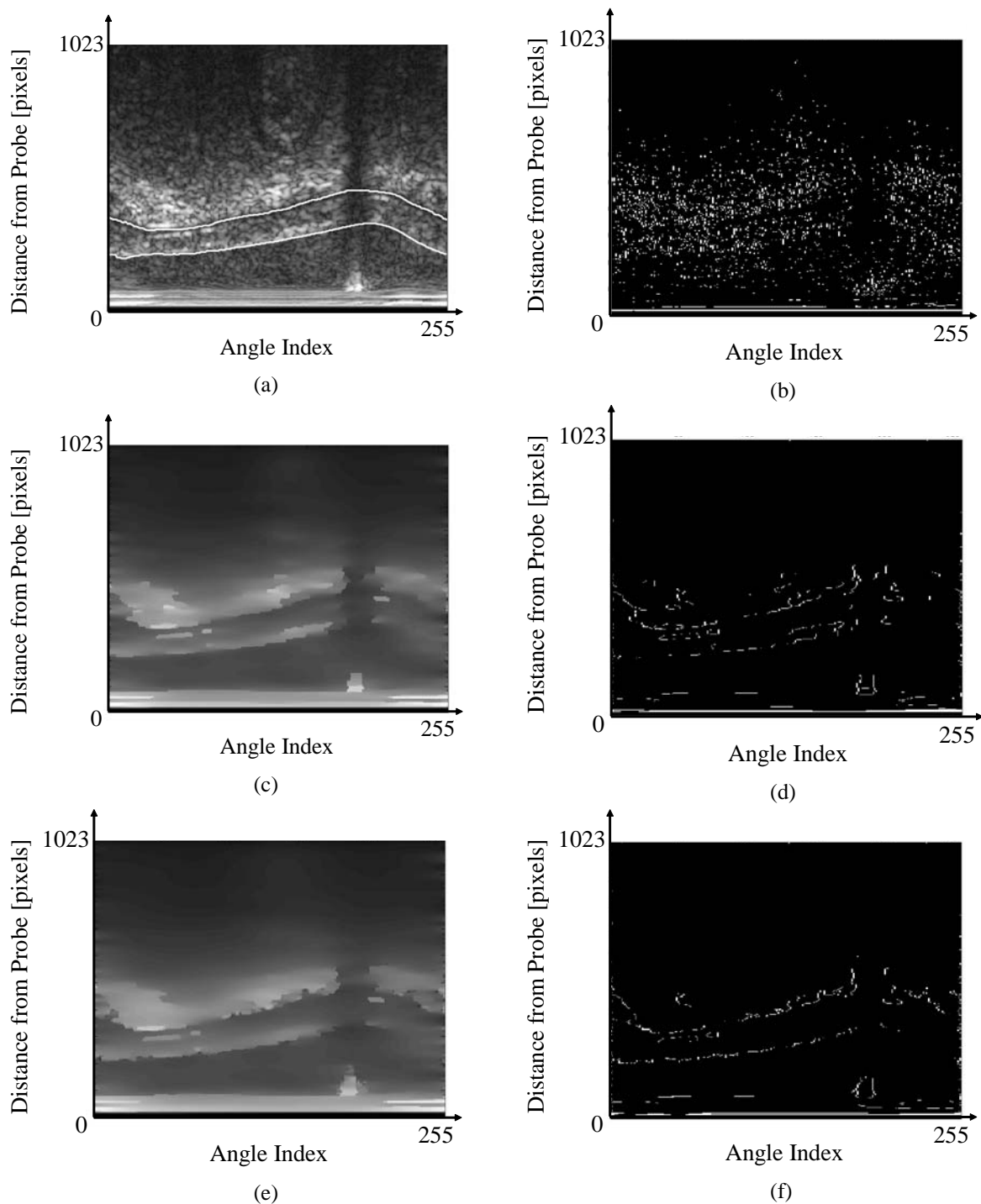


Fig. 7. Experimental results 1. (a) The original image to be processed. The white lines indicate the desirable boundaries to be extracted. (b) Sobel filtering result for Fig.7(a). (c) Edge-preserved smoothing result by the conventional PMD for Fig.7(a) (best result converged at $n=500$). (d) Sobel filtering result for Fig.7(c). (e) Edge-preserved smoothing result by the proposed WSC-PMD for Fig.7(a) (best result converged at $n=1000$). (f) Sobel filtering result for Fig.7(e).

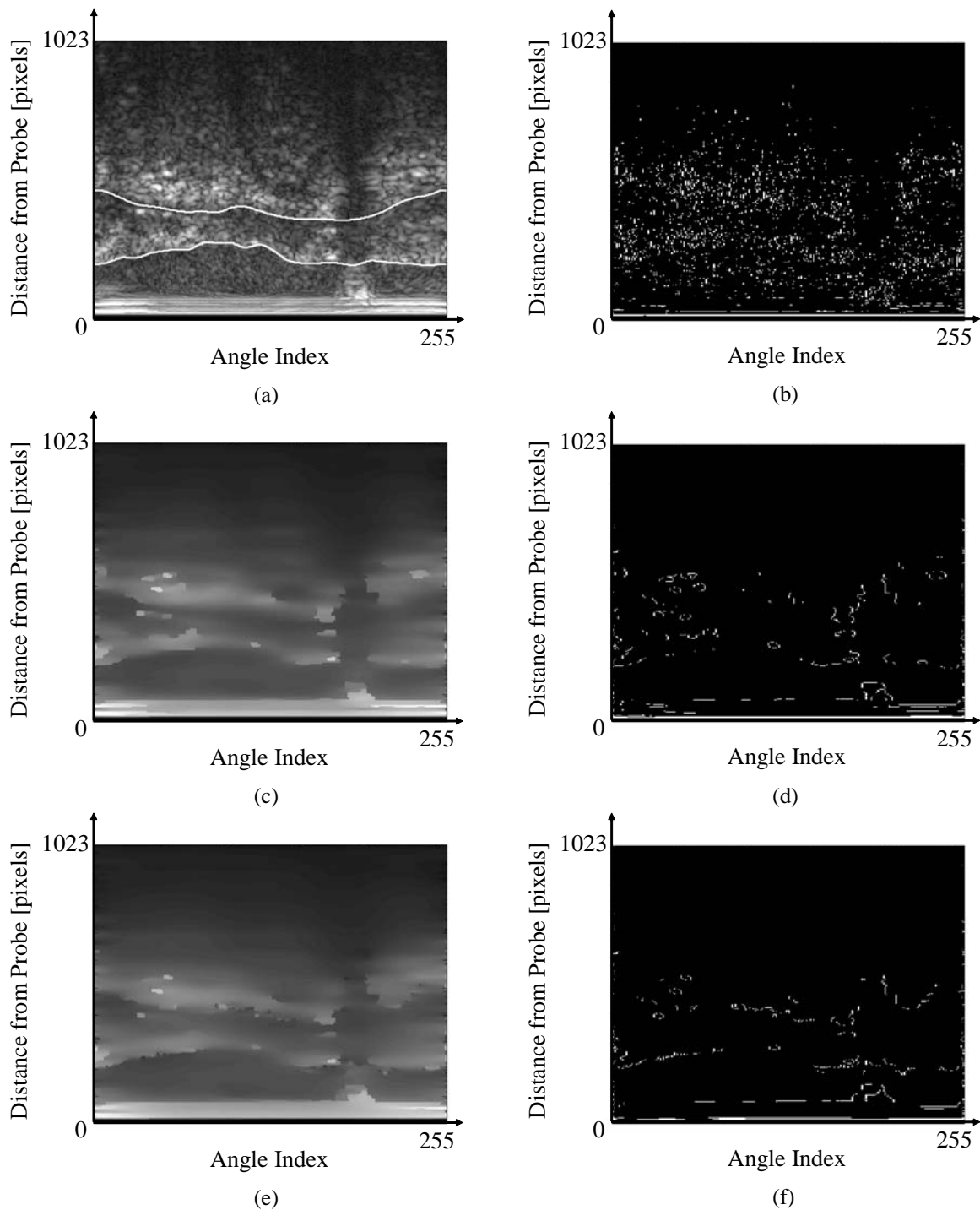


Fig. 8. Experimental results 2. (a) The original image to be processed. The white lines indicate the desirable boundaries to be extracted. (b) Sobel filtering result for Fig.8(a). (c) Edge-preserved smoothing result by the conventional PMD for Fig.8(a) (best result converged at $n=400$). (d) Sobel filtering result for Fig.8(c). (e) Edge-preserved smoothing result by the proposed WSC-PMD for Fig.8(a) (best result converged at $n=1000$). (f) Sobel filtering result for Fig.8(e).

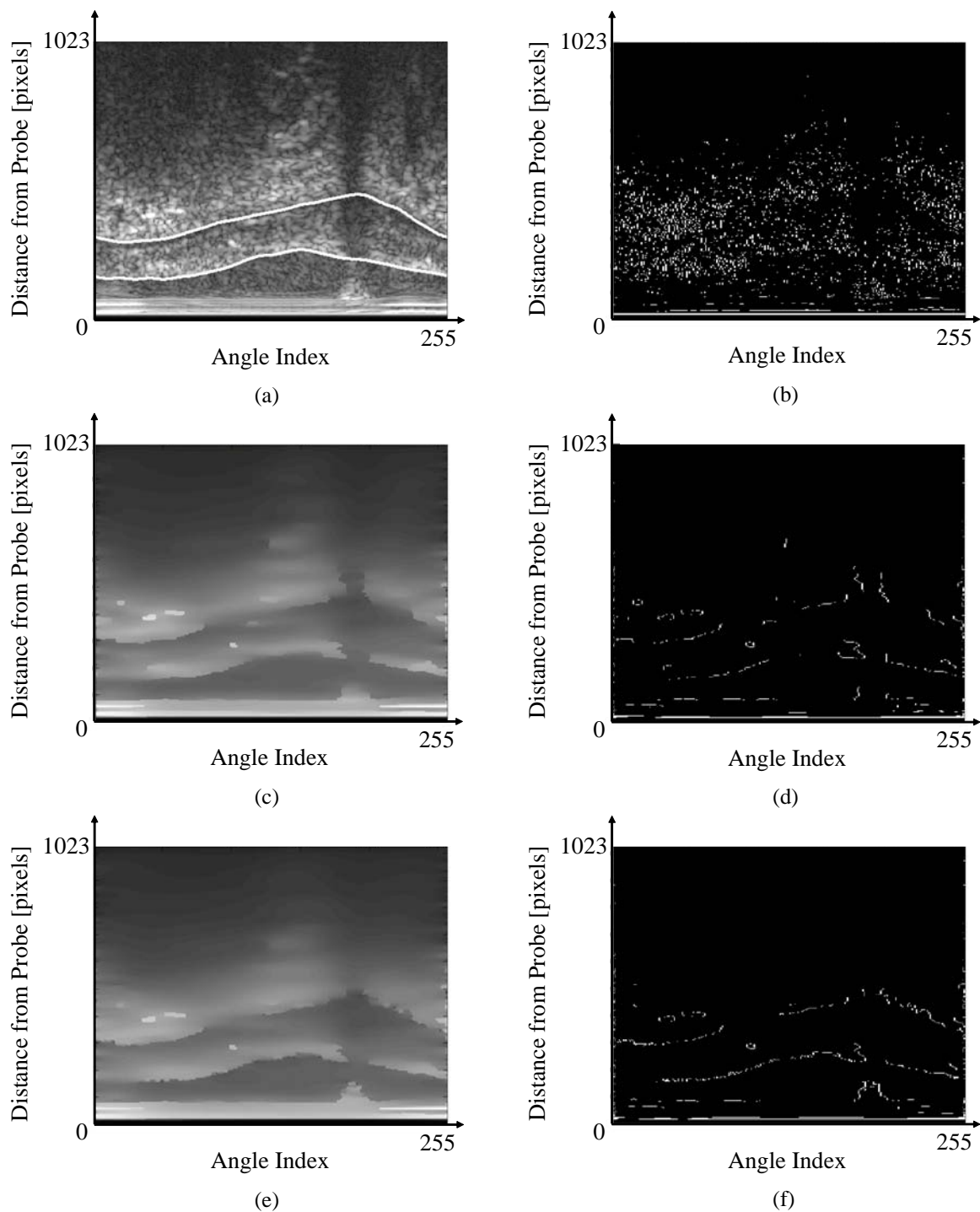


Fig. 9. Experimental results 3. (a) The original image to be processed. The white lines indicate the desirable boundaries to be extracted. (b) Sobel filtering result for Fig.9(a). (c) Edge-preserved smoothing result by the conventional PMD for Fig.9(a) (best result converged at $n=600$). (d) Sobel filtering result for Fig.9(c). (e) Edge-preserved smoothing result by the proposed WSC-PMD for Fig.9(a) (best result converged at $n=1000$). (f) Sobel filtering result for Fig.9(e).

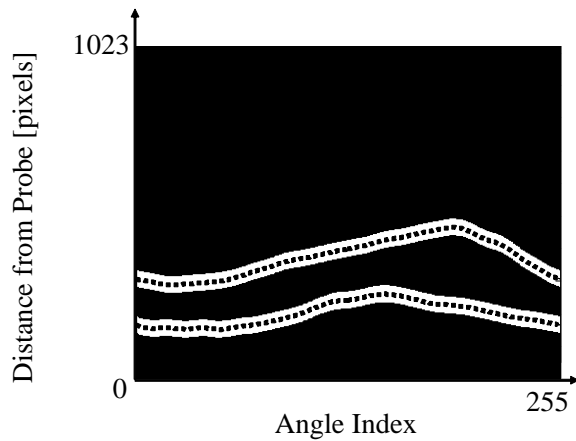


Fig. 10. The subject and the background areas. The dotted lines indicate the desirable plaque boundaries to be extracted. The white region is a subject area for calculating SAV. The black region is a background area for calculating BAV.

image. \bar{I}_1 and \bar{I}_2 are the means of the intensities in the regions 1 and 2, respectively.

Fig.6(b) shows a discriminant image of Fig.3(b) by using η_s^w . Comparing Fig.6(b) by η_s^w with Fig.6(a) by η_s , Fig.6(b) shows vividly the two candidates of plaque boundary. Furthermore, it is observed that the weighted separability in the area where the blood speckle noise exists (in the lumen area) is suppressed.

By modifying the original PMD, the proposed iteration formula of diffusion is given as follows:

$$I_s^{(n+1)} = I_s^{(n)} + \frac{\lambda(1 - \eta_s^w)}{|\phi_s|} \sum_{p \in \phi_s} g(\nabla I_{s,p}^{(n)}) \cdot \nabla I_{s,p}^{(n)}. \quad (12)$$

In the proposed PMD, the diffusion becomes sluggish in the area where the weighted separability is high.

IV. EXPERIMENTAL RESULTS

The proposed method is applied to three real 1024×256 IVUS B-mode images shown in Figs.7(a), 8(a) and 9(a). Those three images are obtained from human patients in vivo, and thus blood speckle noise is observed on each image. In the experiments, the edge-preserved smoothing performance of the conventional PMD and the proposed PMD (weighted separability controlled PMD abbreviated as WSC-PMD) are compared. In all the experiments, the parameters are set to be $K=4$, $\lambda=1.0$, $M_H=70$ and $M_W=3$.

Figs.7(c), 8(c) and 9(c) show the results obtained by the conventional PMD for Figs.7(a), 8(a) and 9(a), respectively. Figs.7(e), 8(e) and 9(e) show the results obtained by the proposed WSC-PMD. It is observed that, comparing with the conventional PMD, the proposed WSC-PMD reduces the speckle noise and enhances the plaque boundaries.

Figs.7(b), (d), (f), 8(b), (d), (f), and 9(b), (d), (f) show the Sobel filtering results for Figs.7(a), (c), (e), 8(a), (c), (e), and 9(a), (c), (e), respectively. It is seen that the pre-processing by the proposed WSC-PMD is better than that by the conventional

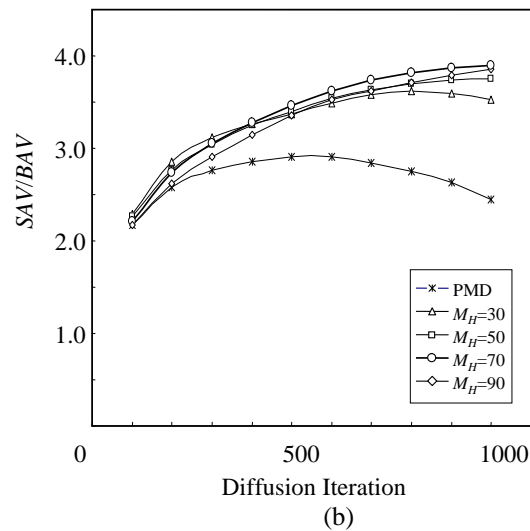
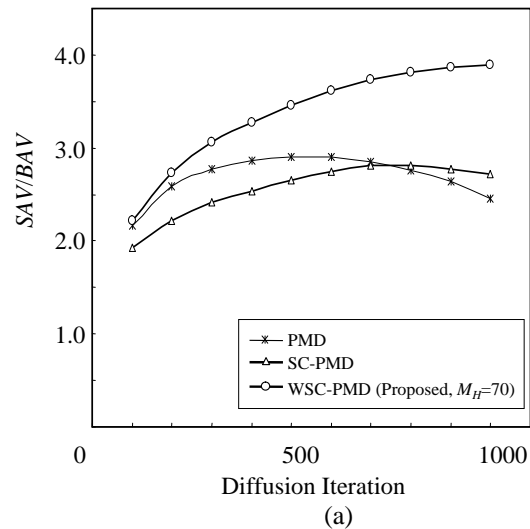


Fig. 11. Smoothing performance for Fig.7(a). (a) SAV/BAV vs. diffusion iteration by each method ($M_H=70$, $K=4$). (b) SAV/BAV vs. diffusion iteration of the proposed method (WSC-PMD) by changing M_H ($K=4$).

PMD for the Sobel filter to detect the edges of the true plaque boundaries. If we employ more suitable edge-detection method other than Sobel filter, the effectiveness of the present WSC-PMD will become more conspicuous.

In order to evaluate quantitatively the performance of edge-preserved smoothing, we use the indices of the Subject Area Variance (SAV) and the Background Area Variance (BAV). SAV and BAV are the means of local variances of subject area and background area, respectively. The variances are calculated with a 9×9 local size window. The subject area is defined to be an area with 25 pixels in depth direction from each side of the desirable plaque boundary. The background area is defined to be an area with the pixels other than those pixels in the subject area. Fig.10 shows the desirable plaque boundaries, the subject area and the background area.

The more the boundaries are enhanced, the more the SAV increases. The more the noises are reduced, the more the BAV decreases. Figs.11(a), 12(a) and 13(a) show the ratio of

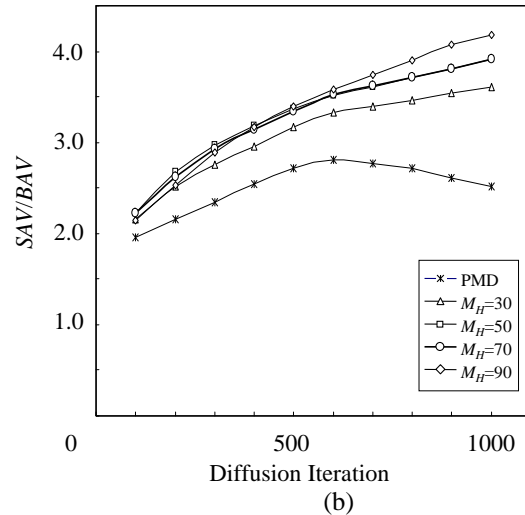
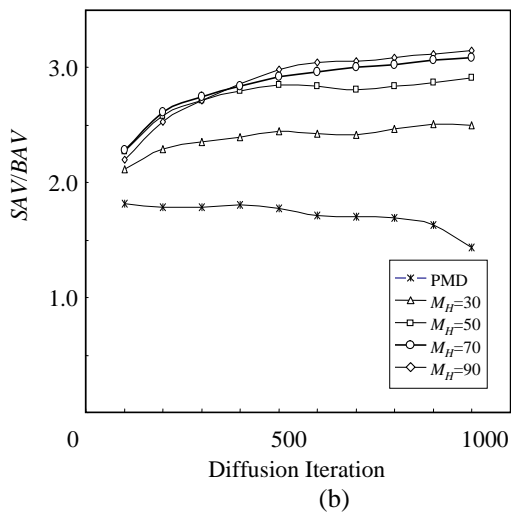
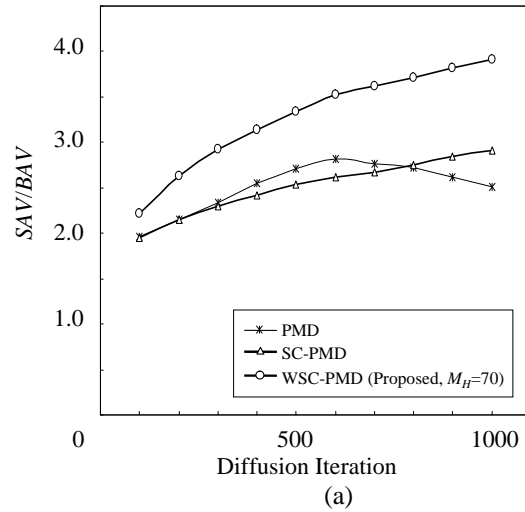
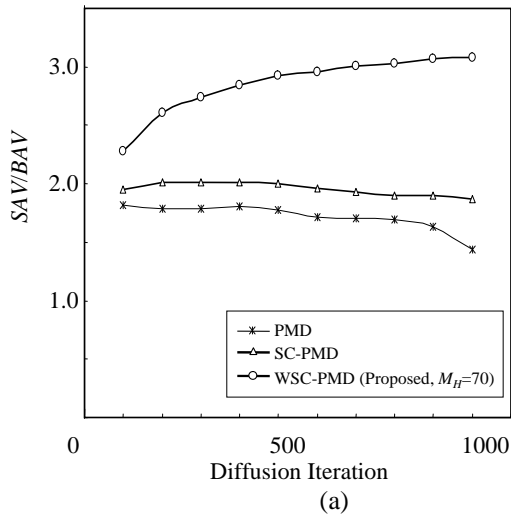


Fig. 12. Smoothing performance for Fig.8(a). (a) SAV/BAV vs. diffusion iteration by each method ($M_H=70$, $K=4$). (b) SAV/BAV vs. diffusion iteration of the proposed method (WSC-PMD) by changing M_H ($K=4$).

Fig. 13. Smoothing performance for Fig.9(a). (a) SAV/BAV vs. diffusion iteration by each method ($M_H=70$, $K=4$). (b) SAV/BAV vs. diffusion iteration of the proposed method (WSC-PMD) by changing M_H ($K=4$).

SAV/BAV for the smoothed images of Figs.7(a), 8(a) and 9(a), respectively. In each figure, the results by using the conventional PMD (abbreviated as PMD), the normal separability controlled PMD (abbreviated as SC-PMD), and the weighted separability controlled PMD (abbreviated as WSC-PMD), are shown. Using the proposed WSC-PMD, SAV/BAV takes large values from an early stage of diffusion process compared with other methods.

In the proposed WSC-PMD, the size M_H of the region for evaluating the weighted separability has an influence on the performance. Figs.11(b), 12(b) and 13(b) show the results of SAV/BAV vs. diffusion iteration of the proposed WSC-PMD by changing M_H .

With those experimental results the effectiveness of the proposed method has been verified.

V. CONCLUSION

In this paper, we have proposed a novel pre-processing method for an edge detection of coronary plaque tissue on

an IVUS image. The present method realizes an efficient edge-preserved smoothing by using an anisotropic diffusion, controlled by a weighted separability of an IVUS image. The present method not only reduces the speckle noise but also enhances the edge of the plaque tissue at the same time. The effectiveness of the proposed method has been confirmed by applying it to the edge-preserved smoothing using the real IVUS images.

The combination of our present method with various kinds of boundary extraction methods is our future study in order to realize a fast and more precise boundary extraction of coronary plaque tissue.

REFERENCES

- [1] M. K. Choong, R. Logeswaran, Z. Musa and A. Ali, "Comparison of monitors for digital diagnosis of medical images," *WSEAS Trans. on Biology and Biomedicine*, vol. 1, pp. 47–50, 2004.
- [2] M. C. Luculescu and S. Lache, "Computer-aided diagnosis system for retinal diseases in medical imaging," *WSEAS Trans. on Systems*, vol. 7, pp. 264–276, 2008.

- [3] P. Galanopoulos, G. Mandellos, G. Anastassopoulos and D. Lymperopoulos, "WCL-Viewer: An integrated system for medical image administration and processing," *WSEAS Trans. on Computers* vol. 3, pp. 1247–1252, 2004.
- [4] G. J. Friedrich, N. Y. Moes, V. A. Muhlberger, C. Gabl, G. Mikuz, D. Hausmann, P. J. Fitzgerald and P. G. Yock, "Detection of intralumenal calcium by intracoronary ultrasound depends on the histologic pattern," *Am Heart J.*, vol. 128, pp. 435–441, 1994.
- [5] B. N. Potkin, A. L. Bartorelli, J. M. Gessert, R. F. Neville, Y. Almagor, W. C. Roberts and M. B. Leon, "Coronary artery imaging with intravascular high-frequency ultrasound," *Circulation*, vol. 81, pp. 1575–1585, 1990.
- [6] J. M. Tobis, J. Mallery, D. Mahon, K. Lehmann, P. Zalesky, J. Griffith, J. Gessert, M. Moriuchi, M. McRae and M. L. Dwyer, "Intravascular ultrasound imaging of human coronary arteries in vivo: Analysis of tissue characterizations with comparison to in vitro histological specimens," *Circulation*, vol. 83, pp. 913–926, 1991.
- [7] S. J. Nicholls, E. M. Tuzcu, I. Sipahi, P. Schoenhagen and S. E. Nissen, "Intravascular ultrasound in cardiovascular medicine," *Circulation*, vol. 114, pp. 54–59, 2006.
- [8] J. B. Hodgson, S. P. Graham, A. D. Savakus, S. G. Dame, D. N. Stephens, P. S. Dhillon, D. Brands, H. Sheehan, M. J. Eberle, "Clinical percutaneous imaging of coronary anatomy using an over-the-wire ultrasound catheter system," *Int. J. Cardiac Imaging*, vol. 4, pp. 187–193, 1989.
- [9] D. T. Linker, A. Klevan, Å. Grønningsether, P. G. Yock, B. J. A. J. Angelsen, "Tissue characterization with intra-arterial ultrasound: Special promise and problems," *Int. J. Cardiac Imaging*, vol. 6, pp. 255–263, 1991.
- [10] M. Kawasaki, H. Takatsu, T. Noda, K. Sano, Y. Ito, K. Hayakawa, K. Tsuchiya, M. Arai, K. Nishigaki, G. Takemura, S. Minatoguchi, T. Fujiwara and H. Fujiwara, "In vivo quantitative tissue characterization of human coronary arterial plaques by use of integrated backscatter intravascular ultrasound and comparison with angioscopic findings," *Circulation*, vol. 105, pp. 2487–2492, 2002.
- [11] K. Sano, M. Kawasaki, M. Okubo, H. Yokoyama, Y. Ito, I. Murata, T. Kawai, K. Tsuchiya, K. Nishigaki, G. Takemura, S. Minatoguchi, X. Zhou, H. Fujita and H. Fujiwara, "In vivo quantitative tissue characterization of angiographically normal coronary lesions and the relation with risk factors: A study using integrated backscatter intravascular ultrasound," *Circulation*, vol. 69, pp. 543–549, 2005.
- [12] E. Falk, "Why do plaques rupture?," *Circulation*, vol. 86 (Suppl III), pp. 30–42, 1992.
- [13] E. Falk, P. K. Shah and V. Fuster, "Coronary plaque disruption," *Circulation*, vol. 92, pp. 657–671, 1995.
- [14] S. E. Nissen, J. C. Gurley, C. L. Grines, D. C. Booth, R. McClure, M. Berk, C. Fischer and A. N. DeMaria, "Intravascular ultrasound assessment of lumen size and wall morphology in normal subjects and patients with coronary artery disease," *Circulation*, vol. 84, pp. 1087–1099, 1991.
- [15] J. D. Klingensmith, D. G. Vince, B. D. Kuban, R. Shekhar, E. M. Tuzcu, S. E. Nissen and J. F. Cornhill, "Assessment of coronary compensatory enlargement by three-dimensional intravascular ultrasound," *Int. J. Cardiac Imaging*, vol. 16, pp. 87–98, 2000.
- [16] J. Ferguson, "Multivariable curve interpolation," *J. of the Association for Computing Machinery*, vol. 11, pp. 221–228, 1967.
- [17] J. H. Ahlberg, E. N. Nilson and J. L. Walsh, *The theory of splines and their applications*, Academic Press, New York, 1967.
- [18] R. Kubota, S. Ichiyama, N. Suetake, E. Uchino, G. Hashimoto, T. Hiro and M. Matsuzaki, "Fuzzy rule-based boundary extraction of plaque in intravascular ultrasound image," *Proc. of the 2008 IAENG Int. Conf. on Imaging Eng.*, pp. 597–600, 2008.
- [19] R. Kubota, N. Suetake, E. Uchino, G. Hashimoto, T. Hiro, and M. Matsuzaki, "Polynomial-based boundary extraction of plaque in intravascular ultrasound image by using its local statistical information," *Innovative Computing, Information and Control Express Letters (ICIC-EL)*, vol. 2, pp. 387–393, 2008.
- [20] M. Sonka, X. Zhang, M. Siebes, M. S. Bissing, S. C. DeJong, S. M. Collins, C. R. McKay, "Segmentation of intravascular ultrasound images: A knowledge-based approach," *IEEE Trans. on Medical Imaging*, vol. 14, pp. 719–732, 1995.
- [21] J. C. Russ, *The Image Processing Handbook*, 5th ed. Academic Press, New York, 2006.
- [22] P. Soille, *Morphological Image Analysis: Principles and Applications*, Springer-Verlag, Telos, 1999.
- [23] C. Tomasi and R. Manduchi, "Bilateral filtering for gray and color images," *Proc. of the 6th Int. Conf. on Computer Vision*, pp. 839–846, 1998.
- [24] P. Perona and J. Malik, "Scale-space and edge detection using anisotropic diffusion," *IEEE Pattern Anal. Mach. Intell.*, vol. 12, pp. 629–639, 1990.
- [25] S. Kim, "Equalized net diffusion (END) in image denoising," *Proc. of the 10th WSEAS Int. Conf. on Applied Mathematics*, pp. 349–354, 2006.
- [26] S. K. Weeratunga and C. Kamath, "Comparison of PDE-based nonlinear anisotropic diffusion techniques for image denoising," *Proc. of SPIE Electronic Imaging, Image Processing: Algorithms and Systems II*, p. 5014, 2003.
- [27] G. J. M. Parker and J. A. Schnabel, "Enhancement of anisotropic diffusive filtering of MR images using approximate entropy," *Proc. of Int. Society for Magnetic Resonance in Medicine*, p. 175, 1999.
- [28] J. Song and H. R. Tizhoosh, "Fuzzy anisotropic diffusion: A rule based approach," *Proc. of the 7th World Multiconference on Systemics, Cybernetics and Informatics*, pp. 241–246, 2003.
- [29] A. Taki, Z. Najafi, A. Roodaki, S. Setarehdan, R. Zoroofi, A. Konig and N. Navab, "Automatic segmentation of calcified plaques and vessel borders in IVUS images," *Int. Journal of Computer Assisted Radiology and Surgery*, vol. 3, pp. 347–354, 2008.
- [30] H. Yoshioka and M. Yuasa, "Heart wall contour extraction on ultrasound images using the automated contour tracking (ACT) method," *Medical Imaging Technology*, vol. 15, pp. 42–50, 1997.
- [31] K. Fukui, "Edge extraction method based on separability of image features," *IEICE Trans. on Inf. and Syst.*, vol. E78-D, pp. 1533–1538, 1995.